A Comprehensive Model for AP-Based Composite Propellant Ignition

M. Kumar,* J. E. Wills,† A. K. Kulkarni,‡ and K. K. Kuo§
The Pennsylvania State University, University Park, Pennsylvania

A comprehensive model and numerical solutions for ignition of AP-based composite solid propellants are presented. The analysis simulates the ignition process of a propellant sample, located in a stagnation region, under rapid pressure loading conditions. Specific features considered in the model include: 1) detailed chemical kinetics information for the ignition of AP-based composite propellants, 2) two-dimensional (axisymmetric) geometry for the composite propellant, and 3) rapid pressurization of the gas phase. An implicit finite difference scheme is used to solve the set of transient, second-order, coupled, inhomogeneous, nonlinear, governing partial differential equations. Numerical solutions reveal a number of important events occurring during the ignition sequence, including: igniter gas penetration to the region near the sample surface, combustion of unburned species upon arrival of compression waves, heat transfer to the propellant, pyrolysis of the oxidizer and fuel, and gas-phase reactions leading to ignition. The model correctly predicts the experimental observation that the ignition delay time decreases as the pressurization rate is increased. The various ignition criteria considered show the same trend as that measured experimentally.

Nomenclature

c, c_p = specific heat
$\mathfrak{D}$ = binary mass diffusion coefficient
E = activation energy
G = external radiation heat flux
I_z = local radiation flux at z
IC = ignition criterion
k = thermal conductivity
k_i = rate constants for reaction i
L = thickness of oxidizer pellet
m = constant defined in Eq. (31)
P = pressure
$\dot{q}''$ = heat flux (energy per unit time per unit area)
$\dot{q}'''$ = heat generation rate (energy per unit time per unit volume)
Q_{py} = heat of pyrolysis per unit mass
r = radial distance from center of statistically averaged element
r_b = burning rate
R = gas constant
R_u = universal gas constant
R_1, R_2 = radii of outer surfaces of oxidizer particle and fuel binder, respectively
t = time
T = temperature
v_z = gas-phase velocity in z direction
$\tilde{W}$ = average molecular weight
Y_j = mass fraction of species j in gas phase
z = distance from initial ($t=0$) position of interface; positive in gas phase
Z = pre-exponential factor
α = radiation absorptivity of interface
β = in-depth radiation absorption coefficient
ρ = density
τ = transmissivity of solid phase
$\dot{\omega}''$ = mass production rate per unit area
$\dot{\omega}_j'''$ = mass production rate per unit volume

Subscripts

1,2,3,4,5 = various reactions of species
F = fuel
F-g = fuel-gas interface
g = gas phase
i = initial value or species i
Ox = oxidizer
Ox-F = oxidizer-fuel interface
Ox-g = oxidizer-gas interface
py = pyrolysis
rad = radiation
s = solid phase
s-g = solid-gas interface
z = axis normal to propellant surface

Presented as Paper 81-1109 at the AIAA/SAE/ASME 18th Joint Propulsion Conference, Cleveland, Ohio, June 21-23, 1982; submitted Sept. 3, 1982; revision submitted March 28, 1983.

*Assistant Professor, Department of Mechanical Engineering; presently, Research Engineer, Gulf Research and Development Company, Pittsburgh, Pa. Member AIAA.

†Research Assistant, Department of Mechanical Engineering; presently with Naval Ordnance Station, Indian Head, Md. Member AIAA.

‡Assistant Professor, Department of Mechanical Engineering.

§Professor, Department of Mechanical Engineering. Associate Fellow AIAA.

Introduction

EXPERIMENTAL investigations on the ignition of composite propellants have shown that under rapid pressure loading conditions a propellant specimen can be ignited in a submillisecond time interval.[1,2] The ignition delay time was observed to depend strongly on the rate of pressurization. The propellant sample was located at the tip of an inert crack. Pressure loading was achieved by high-temperature, high-pressure gases obtained from a solid-propellant igniter system.[1,2] Operating conditions for these experiments were similar to those encountered in the early phase of the transition to detonation in damaged solid-propellant grains. Therefore, an understanding of the ignition mechanism of propellants under these operating conditions can provide insight into and interpretation of the evolution of deflagration-to-detonation transition (DDT).

Ignition of solid propellants has been studied extensively in the past. Detailed reviews of literature on solid-propellant ignition were conducted by Price et al.[3] and more recently by Kulkarni et al.[4] Most of the previous theories consider one-dimensional geometry and can be classified into solid-phase,

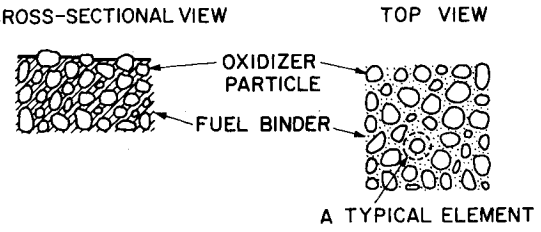

Fig. 1 Schematic diagram of a typical composite propellant structure.

gas-phase, or heterogeneous theory. However, the actual ignition process is, in general, too complex to be described by either gas-phase, solid-phase, or heterogeneous theory under most operating conditions. Bradley[5] proposed a one-dimensional theory that allowed simultaneous reactions in all regions; however, only two very simplified cases were solved. Kumar and Hermance[6] have developed a two-dimensional gas-phase theory, which was the only solid-propellant ignition model considering two-dimensional geometric effects, yet they assumed that both the condensed fuel and the oxidizer have identical thermal properties. None of the existing theories, however, considers ignition under rapid pressurization conditions, which is typical of ignition transients in rocket motors, or the onset of the DDT process in confined, damaged propellant grains. Kumar and Kuo[7] investigated the ignition of the solid-propellant crack tip under pressurization, but they did not consider any gas-phase reactions.

It is apparent that in order to understand the ignition process in detail and to accurately predict the ignition delay time, a comprehensive theoretical model is needed. Specific objectives of this study are:

1) To develop a theoretical model and to obtain numerical solutions for the ignition of AP-based composite solid propellants under rapid pressure loading.

2) To study the effect of such parameters as the pressurization rate and the oxidizer particle size on the ignition process.

3) To validate the theoretical model by comparing predicted results with experimental data.

4) To examine the effect of various ignition criteria on predicted results.

5) To achieve a better understanding of the ignition mechanism under transient pressure loading conditions.

Analysis

Description of Physical Model

The model simulates ignition of a composite propellant in a stagnation region, such as that encountered during the ignition of a propellant located at the tip of a crack or in the circumferential slots of propellant grains. The physical processes that lead to ignition are as follows. Hot combustion product gases from the igniter or main chamber flow into the crack cavity and pressurize it. This causes the pressure of the gases adjacent to the propellant surface to increase rapidly. As the process continues, energy is transferred from the hot gases to the propellant. Following a period of inert heating, the propellant starts to decompose. The fuel and oxidizer species evolved from the surface diffuse and mix with the surrounding gases. In the gas phase, the oxidizer species (evolved from the surface as well as those present in the crack cavity) react with the fuel species; at the same time, surface and/or subsurface reactions in the solid phase continue. When the net heat evolved from the chemical reactions overcomes the heat losses (from subsurface heating, endothermic pyrolysis, etc.), the temperature begins to rise. Eventually, ignition, characterized by a high rate of chemical reactions and heat release, is achieved. The time from the start of the external stimulus to the instant of ignition is defined as ignition delay.

The physical model considers an oxidizer particle embedded in a fuel binder matrix. In an actual composite propellant, oxidizer particles of random size (within a certain range) are distributed in a fuel binder. Figure 1 shows a side cross section and a top view of a typical unimodal composite propellant. For mathematical simulation of this type of propellant, the shape of the oxidizer particles is approximated by a cylindrical pellet of radius R_1 and thickness L, enveloped by a fuel binder of radius R_2, as schematically shown in Fig. 2. The size of the particle and the surrounding binder are determined statistically from the oxidizer particle size distribution and the fuel/oxidant ratio of the propellant. Since the fuel oxidizer unit shown in Fig. 2 is a representative one, the outer boundary at R_2 can be considered adiabatic due to symmetry. Compatible with the solid phase, the adjacent gas phase is also cylindrical with the adiabatic boundary at R_2. Pressurization in the gas phase starts at time $t=0$. Kumar and Hermance[6] employed a similar configuration except that the oxidizer and fuel elements were both infinitely long. When the thermal wave penetration depth is short as compared to the AP particle length (L), the two geometries become equivalent.

Basic Assumptions

The following basic assumptions are employed in the mathematical model:

1) The solid propellant and the gas phase are two-dimensional axisymmetric.

2) The gas-phase pressure is a prescribed function of time and is uniform in a small region adjacent to the solid propellant.

3) Gases obey the perfect gas law.

4) Chemical reactions and pyrolysis processes can be described by the Arrhenius expressions.

5) Binary diffusion coefficients of all species are equal.

6) Prior to ignition, displacement of the propellant surface due to regression can be neglected.

7) The radial bulk velocity is much smaller than the axial.

The assumption of a two-dimensional geometry closely represents a composite propellant, while being mathematically tractable. The gas-phase pressure-time (P-t) relationship is assumed to be known either from a measured P-t trace or a prescribed P-t information simulating an ignition process. Because the pressure is usually not extremely high during the ignition interval, the perfect gas law can be used as the equation of state. Assumptions 4 and 5 are commonly used in combustion models. Assumption 6 is justified for the physical situation of this study. An order-of-magnitude analysis near the tip of a crack shows that bulk radial velocities are, in general, much smaller than bulk axial velocities.

Governing Equations

The mathematical model consists of governing equations for the solid-phase and gas-phase regions. In the solid phase, two energy equations are considered: one for the oxidizer and the other for the fuel. Source terms in these equations include contributions due to in-depth radiation absorption and pyrolysis. The energy equations are coupled to the gas-phase conservation equations through the heat flux balance at the solid-gas interface. Gas-phase behavior is described by mass, energy, and species conservation equations. A measured pressure-time trace near the propellant sample surface is considered as input to the model. For the AP-based propellant, five different species (NH_3, $HClO_4$, gaseous fuel, gaseous oxidizer, and products) are considered to be present in the gas phase.

For the coordinates shown in Fig. 2, transient heat conduction equations for the oxidizer and fuel binder in the solid phase are

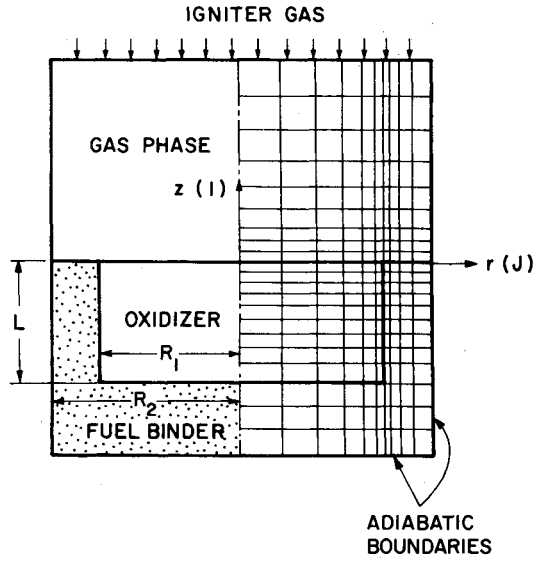

Fig. 2 Schematic cross-sectional view of a statistically averaged element and finite difference grid pattern.

Oxidizer:

$$\rho_{\mathrm{Ox,s}} c_{\mathrm{Ox,s}} \frac{\partial T}{\partial t} = \frac{\partial}{\partial z}\left(k_{\mathrm{Ox,s}} \frac{\partial T}{\partial z}\right) + \frac{1}{r}\frac{\partial}{\partial r}\left(k_{\mathrm{Ox,s}} r \frac{\partial T}{\partial r}\right) + \dot{q}'''_{\mathrm{Ox,s}} \quad (1)$$

Fuel:

$$\rho_{\mathrm{F,s}} c_{\mathrm{F,s}} \frac{\partial T}{\partial t} = \frac{\partial}{\partial z}\left(k_{\mathrm{F,s}} \frac{\partial T}{\partial z}\right) + \frac{1}{r}\frac{\partial}{\partial r}\left(k_{\mathrm{F,s}} r \frac{\partial T}{\partial r}\right) + \dot{q}'''_{\mathrm{F,s}} \quad (2)$$

where

$$\dot{q}'''_{\mathrm{Ox,s}} = \dot{q}'''_{\mathrm{Ox,rad}} + \dot{q}'''_{\mathrm{Ox,py}} \quad (3)$$

$$\dot{q}'''_{\mathrm{Ox,rad}} = \tau_{\mathrm{Ox}} G \beta_{\mathrm{Ox}} e^{-\beta_{\mathrm{Ox}} z} = \beta_{\mathrm{Ox}} I_z \quad (4)$$

and

$$\dot{q}'''_{\mathrm{Ox,py}} = -Z_{\mathrm{Ox,py}} Q_{\mathrm{Ox,py}} \exp(-E_{\mathrm{Ox,py}}/R_u T) \quad (5)$$

The functional form of the pyrolysis heat absorption term in Eq. (5) is the same as that used by Ohlemiller and Summerfield.[8] The expression for $\dot{q}'''_{\mathrm{F,s}}$ is similar to that of $\dot{q}'''_{\mathrm{Ox,s}}$.

The gas-phase consevation equations are

Continuity:

$$\frac{\partial \rho_g}{\partial t} + \frac{\partial(\rho_g v_z)}{\partial z} = 0 \quad (6)$$

Energy:

$$c_p \rho_g \frac{\partial T}{\partial t} + \rho_g c_p v_z \frac{\partial T}{\partial z} - \frac{\partial P}{\partial t} = \frac{\partial}{\partial z}\left(k_g \frac{\partial T}{\partial z}\right) + \frac{1}{r}\frac{\partial}{\partial r}\left(k_g r \frac{\partial T}{\partial r}\right) + \dot{q}_g''' \quad (7)$$

Species:

$$\rho_g \frac{\partial Y_j}{\partial t} + \rho_g v_z \frac{\partial Y_j}{\partial z} = \frac{\partial}{\partial z}\left(\rho_g \mathfrak{D} \frac{\partial Y_j}{\partial z}\right) + \frac{1}{r}\frac{\partial}{\partial r}\left(\rho_g \mathfrak{D} r \frac{\partial Y_j}{\partial r}\right) + \dot{\omega}_j''' \quad (8)$$

where $j=1$, 2, 3, or 4 represents the gas-phase species, oxidizer, NH_3, $HClO_4$, or fuel, respectively.

The inhomogeneous terms $\dot{q}'''$ and $\dot{\omega}'''$ are obtained by using the chemical kinetics information described in a later section.

Since the region of interest in the gas phase during the ignition process is very small (in the order of 1 mm), local pressurein this region is considered to be spatially uniform. (It should be noted that the time for the pressure wave to travel this short distance is two orders of magnitude smaller than the characteristic time for ignition.) However, pressure is allowed to vary with respect to time. Therefore, the gas-phase momentum equations are replaced by the measured pressure,

$$P = P(t) \quad (9)$$

The equation of state for the gas phase is

$$\rho_g = P\bar{W}/R_u T \quad (10)$$

Initial and Boundary Conditions

The initial condition for the solid phase (both fuel and oxidizer) is

$$\text{at } t=0: \quad T(0,r,z) = T_i \quad (11)$$

Boundary conditions for the solid phase are as follows. The temperature far from the interface is the same as the propellant initial temperature, i.e.,

$$\text{at } z \to -\infty: \quad T = T_i \quad (12)$$

Temperature continuity at various interfaces requires

$$T|_{r=R_I^+} = T|_{r=R_I^-} \quad \text{and} \quad T|_{z=-L^-} = T|_{z=-L^+} \quad (13)$$

On symmetric surfaces, the adiabatic conditions are

$$\text{on } r=0: \quad \frac{\partial T}{\partial r} = 0 \quad (14)$$

and

$$\text{on } r=R_2: \quad \frac{\partial T}{\partial r} = 0 \quad (15)$$

At solid-gas and oxidizer-fuel interfaces, heat flux balance gives

$$\text{at } z=z_{\mathrm{s\text{-}g}}: \quad k_s \frac{\partial T}{\partial z}\bigg|_{z_{\mathrm{s\text{-}g}}^-} = k_g \frac{\partial T}{\partial z}\bigg|_{z_{\mathrm{s\text{-}g}}^+} + \alpha_{\mathrm{s\text{-}g}} G + r_{b_s} \rho_s T (c_{p_s} - c_{p_g}) + \dot{q}''_{\mathrm{s\text{-}g}} \quad (16)$$

where $\dot{q}''_{\mathrm{s\text{-}g}}$ is the net heat generation at the surface, and

$$\text{at } z=-L: \quad k_{\mathrm{F,s}} \frac{\partial T}{\partial z}\bigg|_{-L^+} = k_{\mathrm{Ox,s}} \frac{\partial T}{\partial z}\bigg|_{-L^+} + \alpha_{\mathrm{Ox\text{-}F}} \tau_{\mathrm{Ox}} G e^{-\beta_{\mathrm{Ox}} L} \quad (17)$$

$$\text{at } r=R_I \text{ and } -L<z<0: \quad -k_{\mathrm{F,s}} \frac{\partial T}{\partial r}\bigg|_{R_I^+} = -k_{\mathrm{Ox,s}} \frac{\partial T}{\partial r}\bigg|_{R_I^-} \quad (18)$$

Initial conditions for the gas-phase equations (for $j=1,2,3,4$) are

$$\text{at } t=0:\ v_z(0,r,z)=0;\ T(0,r,z)=T_{g,i};\ Y_j(0,r,z)=Y_{j,i} \quad (19)$$

The boundary conditions for the gas phase are as follows. The symmetry conditions at the centerline and outer boundary give

$$\text{on } r=0:\quad \frac{\partial T}{\partial r}=0 \text{ and } \frac{\partial Y_j}{\partial r}=0 \quad (20)$$

and

$$\text{on } r=R_2:\quad \frac{\partial T}{\partial v}=0 \text{ and } \frac{\partial Y_j}{\partial r}=0 \quad (21)$$

Far away from the surface,

$$z\to\infty:\quad \frac{\partial T}{\partial z}=0 \text{ and } \frac{\partial Y_j}{\partial z}=0 \quad (22)$$

The temperature continuity at the interface gives

$$\text{on } z=z_{s\text{-}g}:\quad T|_{z_{s\text{-}g}+}=T|_{z_{s\text{-}g}-} \quad (23)$$

The overall and individual species mass flux balance at the solid-gas interface is given as follows:

$$\text{on } z=z_{s\text{-}g}:\quad \rho_g v_z=\rho_s r_{b_s} \quad (24)$$

and

$$\rho_g v_z Y_j|_{z_{s\text{-}g}-}=\rho_g v_z Y_j|_{z_{s\text{-}g}+}-\rho_g \mathcal{D}\frac{\partial Y_j}{\partial z}-\dot{\omega}_j'' \quad (25)$$

Reaction Kinetics of AP/PBAA Propellant

Very little information is available in the literature to describe the detailed elementary chemical reactions for AP/PBAA propellant ignition or combustion. Consequently, the ignition process is modeled in terms of a number of overall reactions. Kinetic constants for these reactions are estimated with the help of values quoted in the literature. It may be noted that numerical values of the solution depend strongly upon proper knowledge of the chemical kinetic parameters, many of which are unfortunately not known accurately.

It is generally accepted that the decomposition of AP consists of 1) exothermic degradation of AP into gaseous products and 2) endothermic dissociation of AP into gaseous NH_3 and $HClO_4$.[9-14] It is also believed that AP pyrolysis consists of 70% exothermic degradation and 30% dissociative sublimation.[9] The activation energy of this decomposition is estimated to be between 20-30 kcal/mole.[9-14] In the present study, the value was taken at 24 kcal/mole. The activation energy of the premixed reaction between NH_3 and $HClO_4$ is 15.5 kcal/mole.[10] The pyrolysis of the fuel (PBAA) is endothermic. The activation energy for fuel pyrolysis was taken as 113 kJ/mole (27 kcal/mole); Ninan and Krishnan[15] have shown that for many polybutadiene binders the activation energy for thermal decomposition is around 110 kJ/mole. (It may be noted that Varney and Strahle[16] reported the activation energy for PBAA decomposition as 34 kcal/mole.) The pyrolysis products of the fuel and oxidizer react in the gas phase to form the final products; however, no reliable estimate of the kinetic parameters for this reaction is available.

The present investigation considers the following five chemical reactions: 1) exothermic degradation of the solid AP particle into oxidizer gases, 2) dissociative sublimation of AP into NH_3 and $HClO_4$, 3) reaction between premixed NH_3 and $HClO_4$ gases, 4) fuel pyrolysis, and 5) diffusion flame resulting from the chemical reaction between the oxidizer and fuel gases to form products:

$$AP_{(s)} \xrightarrow[\text{exothermic degradation}]{k_1} Ox_{(g)} \quad (26)$$

$$AP_{(s)} \xrightarrow[\text{dissociative sublimation}]{k_2} NH_{3(g)}\,HClO_{4(g)} \quad (27)$$

$$NH_{3(g)}+HClO_{4(g)} \xrightarrow[\text{premixed A/PA reaction}]{k_3} Ox_{(g)} \quad (28)$$

$$PBAA_{(s)} \xrightarrow[\text{pyrolysis}]{k_4} fuel_{(g)} \quad (29)$$

$$Ox_{(g)}+fuel_{(g)} \xrightarrow[\text{diffusion flame}]{k_5} products_{(g)} \quad (30)$$

Modeling of Source Terms

In order to solve the governing equations, the source terms $\dot{q}''$, $\dot{q}'''$, $\dot{\omega}_j'''$, and $\dot{\omega}_j''$ must be expressed as functions of other variables and known parameters. In modeling the source terms, it is implicitly assumed that the rate-controlling reactions are single-step and irreversible. It is further assumed that the reaction rate constants have Arrhenius dependence on local temperature and are given by

$$k=ZT^m\exp(-E/R_uT) \quad (31)$$

If the gas-phase mass fractions Y_1, Y_2, Y_3, Y_4, Y_5 represent the oxidizer, ammonia, perchloric acid, fuel, and products, respectively, the source terms can be expressed as follows:

$$\dot{\omega}_1'''=Z_3\frac{W_1}{W_2W_3}\rho_g^2Y_2Y_3T\exp(-E_3/R_uT)$$
$$-z_5\frac{1}{W_4}\rho_g^2Y_1Y_4\exp(-E_5/R_uT) \quad (32)$$

$$\dot{\omega}_2'''=Z_3\frac{1}{W_3}\rho_g^2Y_2Y_3T\exp(-E_3/R_uT) \quad (33)$$

$$\dot{\omega}_3'''=\dot{\omega}_2'''(W_3/W_2) \quad (34)$$

$$\dot{\omega}_4'''=-Z_5\frac{1}{W_1}\rho_g^2Y_1Y_4\exp(-E_5/R_uT) \quad (35)$$

$$\dot{q}_g'''=(\dot{\omega}_2'''\Delta H_3+\dot{\omega}_4'''\Delta H_5) \quad (36)$$

where ΔH_3 is the heat of reaction per unit mass of ammonia for reaction 3 [Eq. (28)], and ΔH_5 is the heat of reaction per unit mass of fuel for reaction 5 [Eq. (30)]. Since no heterogeneous reactions are considered in the present model, $\dot{\omega}_j''$ is zero and $\dot{q}''$ contains only the heat of pyrolysis. The

values of heat of pyrolysis are given in the table of input parameters (see Table 1 below).

Numerical Solution Procedure

The governing equations, as outline earlier, represent a set of transient, second-order, coupled, inhomogeneous, nonlinear, partial differential equations. An exact analytic solution of this set of equations cannot be obtained. Also, approximate solution methods employing asymptotic expansion or similarity do not appear to be useful. For a complete solution, therefore, the numerical method is used. Several key steps of the solution procedure are briefly described in the following.

Coordinate Transformation

The mathematical domain in $\hat{z}$ direction was mapped into a finite region, using the transformation given below. This transformation makes possible a finer grid size near the propellant surface in the real spatial coordinate, where large temperature gradients exist, while using a uniform grid in the transformed coordinate. The following exponential transformation is used for the axial coordinate:

Solid phase:

$$s=\exp(A_s z)-1 \text{ or } z=(1/A_s)\ell n(1+s) \tag{37}$$

Gas phase:

$$s=1-\exp(-A_g z) \text{ or } z=-(1/A_g)\ell n(1-s) \tag{38}$$

This transforms $z=-\infty,0,\infty$ to $s=-1,0,1$, respectively. The radial coordinates remain unchanged.

Finite Difference Scheme

An implicit finite difference scheme was used to solve the governing equations. A central difference scheme was used to approximate axial derivatives. A three-point variable mesh, Allen's method,[17] was employed to represent radial derivatives, because the conventional central difference scheme does not accurately represent radial derivatives when the radial coordinate is very small. The time derivatives were approximated by a generalized Crank-Nicolson scheme. A quasilinearization technique was used to linearize the inhomogeneous (or source) terms of the governing equations.

The resulting set of simultaneous finite difference equations was solved by a successive over-relaxation iterative scheme.[17] The following checks were made on the computed solutions: 1) comparison of the numerical results with the analytical solutions showed excellent agreement for some simple cases and 2) the computed results also satisfied the global and local energy balances.

It should be noted that for the five species considered in the model, only three species equations must be solved independently, since species 2 and 3 (i.e., ammonia and perchloric acid) can be shown to have identical governing equations and boundary conditions. Mass fraction of products Y_5 is obtained from the following algebraic relation:

$$Y_5=1-\sum_{j=1}^{4} Y_j \tag{39}$$

Results and Discussion

Input Parameters and Initial Conditions

Numerical values of the important input parameters to the computer program are listed in Table 1. Propellant composition, oxidizer particle size, etc., are the same as those for the experimental study.[1,2] Thermal properties of AP were taken from Ref. 18. Thermal properties of PBAA are approximate and are identical to those used by Varney and Strahle.[16] Thermal conductivity of PBAA was deduced from the average density of fuel and the value of thermal diffusivity used in Ref. 16 for fuel binders. Thermal properties for the gas phase were obtained by averaging the thermal properties of the combustion product species of the AP/PBAA propellant. The thermal conductivity is assumed to vary as $T^{0.75}$. The composition of these products species was determined from the NASA Lewis chemical equilibrium calculation program.[19] Molecular weights of the gas-phase species were obtained in a similar fashion. The numerical

Table 1 Physical properties and input parameters

Property	Units	Gas phase	Solid phase	
			AP	PBAA
c	J/kg·K	1922	1305	1255
k	W/m·K	$0.228\,(T/300)^{0.75}$	0.46	0.12
$\mathfrak{D}$	m^2/s	0.2×10^{-4}	—	—
L[a]	μm	—	37.5	—
R_1[a]	μm	—	30.6	—
R_2[a]	μm	—	—	40
ρ	kg/m^3	P/RT	1950	947
W	kg/kmole	$W_1=29.2$, $W_2=17.0$, $W_3=100.5$, $W_4=24.5$, $W_5=20.4$	117.5	100.8

[a] For AP particle size of 76 μm and 75% solids loading.

Table 2 Chemical kinetic constants

Reaction No. [see Eqs. (26-30)]	Activation energy E, J/kmole	Heat of reaction ΔH, J/kg	m [see Eq. (31)]	Order of reaction
1	1.00×10^8	-1.61×10^6	0	0
2	1.00×10^8	2.07×10^6	0	0
3	0.65×10^8	-2.23×10^7	1	2
4	1.13×10^8	2.38×10^5	0	0
5	0.42×10^8	-1.86×10^6	0	2

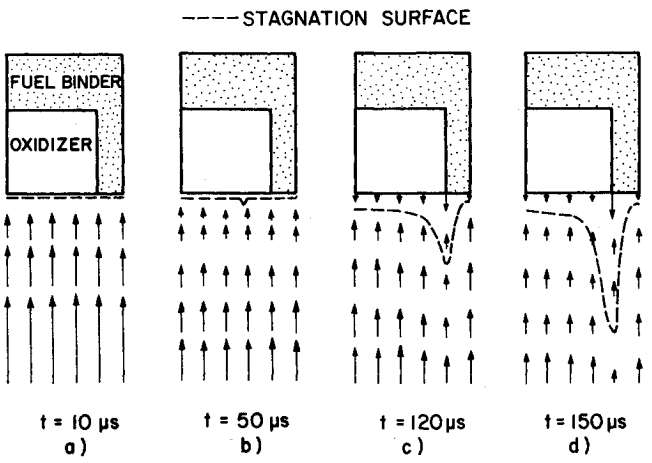

Fig. 3 Schematic of sequential variation of axial velocity field adjacent to propellant surface.

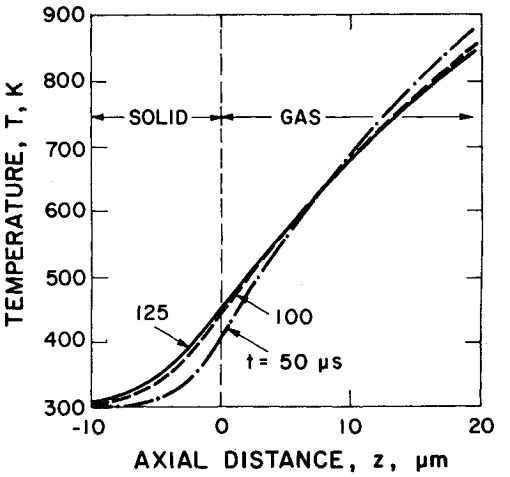

Fig. 5 Axial temperature variation at AP/PBAA interface ($r=R_f$) for various times (average $dP/dt = 120$ GPa/s).

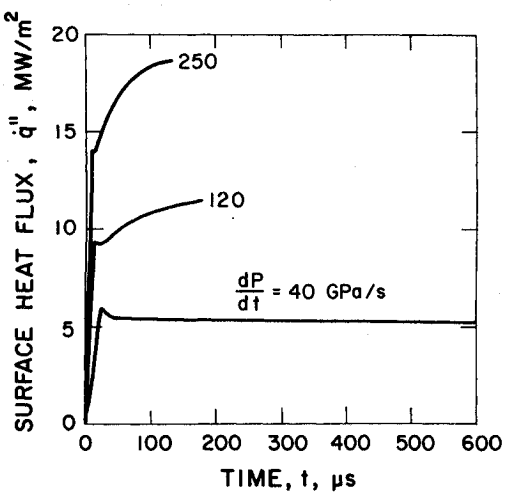

Fig. 4 Calculated time variation of surface heat flux at AP/PBAA interface ($r=R_f$) for various pressurization rates.

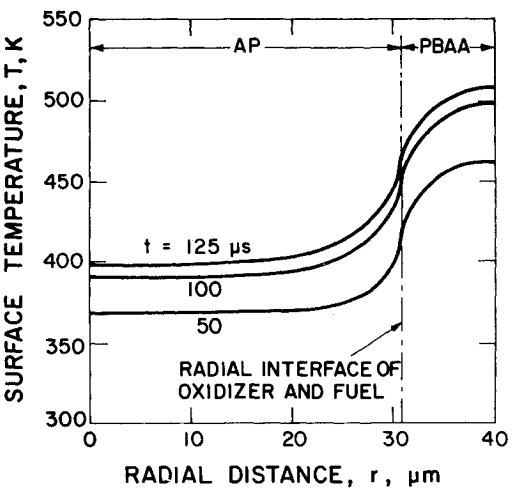

Fig. 6 Radial variation of surface temperature at various times (average $dP/dt = 120$ GPa/s).

values of the chemical kinetic constants are given in Table 2. Some of the activation energies and pre-exponential factors given in Table 2 are approximate, due to lack of kinetic data. It should be noted that the chemical kinetics of ignition may differ significantly from those of steady-state combustion.

The initial conditions for computations were consistent with those encountered in the experiments. The initial pressure and temperature were 0.1 MPa and 300 K, respectively. In order to simulate the bright reaction zone observed near the tip (see Refs. 1 and 2), a mixture of gaseous oxidizers and fuel species was assumed to be present at $t=0$. Experimentally measured pressure-time traces were used as input to the computer program.

Predicted Ignition Sequence

The general sequence of events leading to ignition, as revealed by the numerical solution, is as follows.

As pressurization of the crack cavity begins, the temperature in the crack increases, and the gases flow toward the crack tip at high velocities (see Fig. 3a). The rise in the gas temperature produces a temperature gradient at the solid-gas interface, heat is transferred to the solid propellant, and heating of the solid propellant begins. At the same time, as the gas temperature rises, the initial unreacted oxidizer and fuel species (from the igniter system) react, further increasing the local gas temperature as well as the heat flux to the propellant (see Fig. 4). This results in a continuous increase in the propellant surface temperature during the initial period.

As time progresses, the initial unreacted species present in the gas phase are completely consumed and the temperature of the propellant surface continues to rise. This causes a slight attenuation in the heat flux to the propellant surface. The heat flux increases very rapidly during the initial period and then levels off. The axial temperature distribution at the oxidizer fuel interface ($r=R_f$) at various times is shown in Fig. 5. As seen in Fig. 5, the thermal wave penetration into the solid increases with time. Temperatures far from the surface remain quite uniform.

Since the thermal properties of AP and PBAA are very different, there is a steep temperature gradient near the AP/PBAA interface. Figure 6 shows the radial variation of the propellant surface temperature as a function of time. Because PBAA has a lower thermal diffusivity and conductivity, its surface temperature rises much faster than that of AP. The gas-phase temperature near the propellant surface also changes with the radius and is strongly coupled to the solid-gas interface temperature. Farther away from the propellant surface, the radial gas temperature variation diminishes.

Figure 7 shows time variation of the maximum volumetric gas-phase heat release. The gas-phase reaction between the unburned oxidizer and fuel species lasts for about 10 μs.

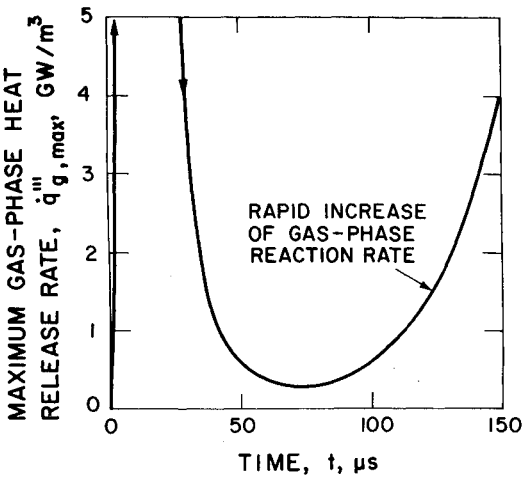

Fig. 7 Calculated time variation of maximum volumetric gas-phase heat release (average $dP/dt = 120$ GPa/s).

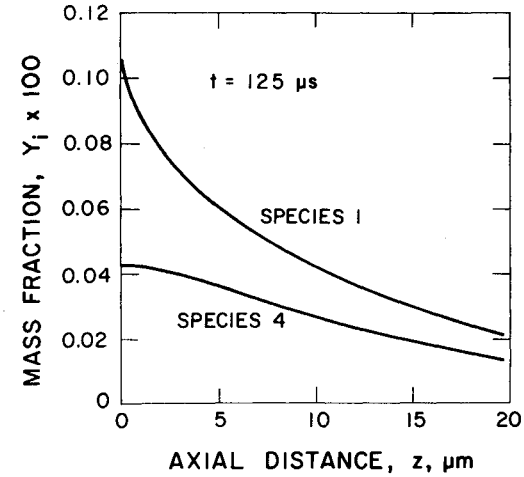

Fig. 9 Axial distribution of oxidizer (Y_1) and fuel (Y_4) species above AP/PBAA interface ($r = R_1$) (average $dP/dt = 120$ GPa/s).

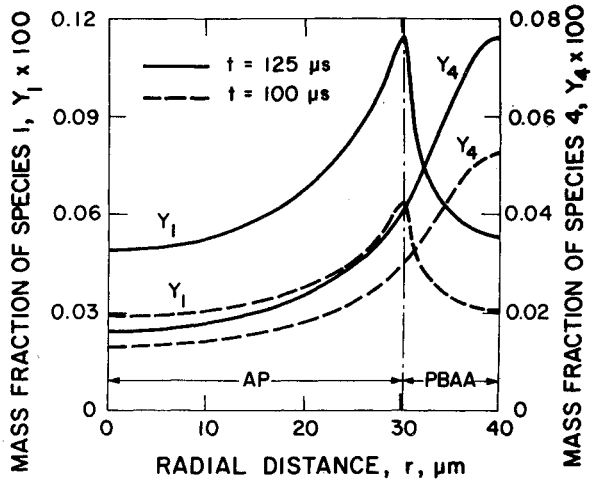

Fig. 8 Radial variation of oxidizer (Y_1) and fuel (Y_4) species mass fraction near the solid-gas interface at two different times (average $dP/dt = 120$ GPa/s).

During this interval the heat release rate is extremely high (the values are off the scale of Fig. 7). The high initial concentration of the species causes the rate of heat generation to increase abruptly as the local temperature increases due to pressurization. The heat generation rate peaks and then drops to almost zero (even though the temperature continues to increase) since the reacting species are consumed rapidly. As time progresses, gas velocities decrease because of the pressure rise in the cavity (see Fig. 3b).

Following a relatively long period of inert heating, the AP and PBAA start to pyrolyze when the propellant surface temperature becomes sufficiently high. The gasified species of oxidizer, fuel, NH_3, and $HClO_4$ diffuse away from the surface, both axially and radially. As shown in Figs. 8 and 9, the concentration of the fuel species is the highest above the surface where $r = R_2$, where the fuel surface temperature is highest (see Fig. 6). The fuel mass fraction decreases away from the location. The oxidizer concentration is highest at the AP-PBAA interface ($r = R_1$), as shown in Figs. 8 and 9, where the AP surface temperature is highest (see Fig. 6). As time progresses, the mixing of fuel and oxidizer species continues because of diffusion and convection. Since local temperatures are not high enough to support vigorous gas-phase reactions, the concentration of these species continues to increase as a result of accumulation.

As the pressurization process continues, the temperature of the gas phase continues to increase. At the same time, there is an accumulation of fuel and oxidizer species due to pyrolysis of the propellant. When the local concentrations and temperature reach suitable values, vigorous gas-phase reaction between the pyrolyzed oxidizer and fuel species ensues (see Fig. 7). Ignition is defined as the attainment of high gas-phase reaction rates (see Fig. 7) and simultaneous high surface pyrolysis rates (see Fig. 3c and 3d).

Parametric Studies

Since there is no universally accepted ignition criterion (IC), several ignition criteria were employed to test the predictive capability of the model. The onset of ignition is defined as the time at which 1) the local maximum of volumetric gas-phase heat release reaches a critical value ($\dot{q}'''_{g,max}$); 2) the AP pyrolysis rate near the radial oxidizer-fuel interface reaches a critical value; 3) the axial gas velocity at $r = R_1$ at a specified distance from the surface is zero (i.e., when the surface blowing is sufficiently large to overcome the incoming gas velocity induced by pressurization of the cavity, as shown in Fig. 3c); 4) the rate of maximum volumetric gas-phase heat release reaches a critical value; or 5) the rate of AP pyrolysis rate reaches a critical value. The critical values were obtained by matching the predicted ignition delay with experimental data for one case. Comparison between predicted ignition delay (for the first three ignition criteria mentioned above) is shown in Fig. 10. It is clear that all three criteria correctly predict the experimentally observed trend that ignition delay time is lower for a higher pressurization rate. The last two criteria also show the same trend.

Predicted ignition delay time shows a greater dependence on the choice of ignition criteria at lower pressurization rates. The criterion based on zero velocity (IC 3) or critical burning rate (IC 2) results in a lower ignition delay time than that based on gas-phase heat release (IC 1). This is reasonable because at a lower pressurization rate the gas-phase temperature increases at a slower rate; therefore, the time lag between significant pyrolysis and the attainment of the critical gas-phase reaction rate is longer. Theoretical results overestimate the ignition delay time at lower pressurization rates and slightly underestimate the ignition delay time at higher pressurization rates (see Fig. 10); this may be caused by the approximate values of the chemical kinetic constants used in the computation. Overall, the predicted results are in reasonable agreement with the measured data.

Another possible ignition criterion that can be used, but which was not employed for the results presented in this paper, is the appearance of an abrupt rise (spike) in the

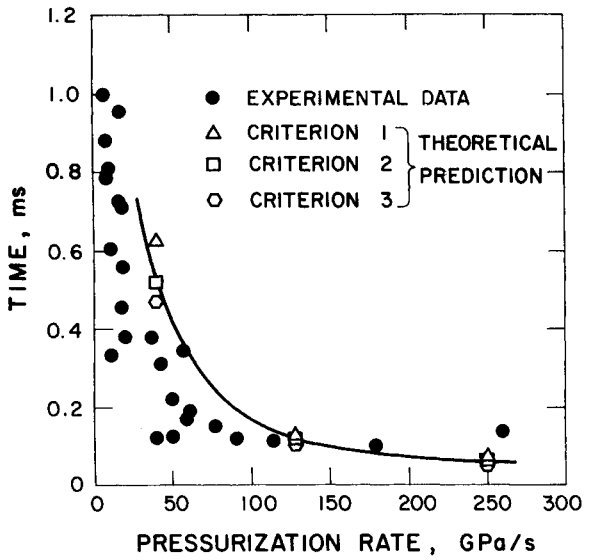

Fig. 10 Comparison of measured and predicted ignition delays using different ignition criteria based upon the attainment of: 1) $\dot{q}'''_{max,critical}$, 2) $r_{b,\,critical}$, and 3) zero axial velocity in the gase phase at a specified location.

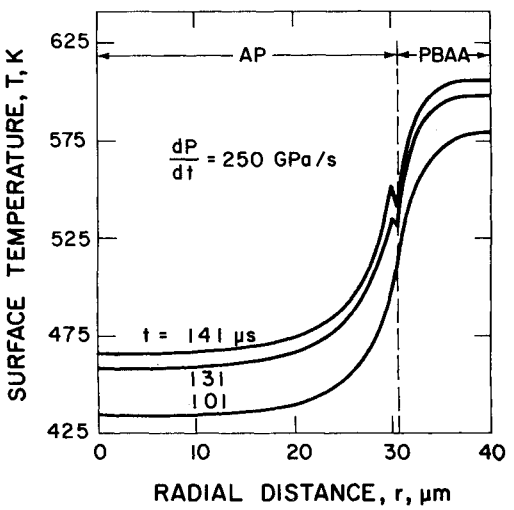

Fig. 11 Radial variation of surface temperature showing the appearance of temperature peaks near the oxidizer-fuel interface.

surface temperature (see Fig. 11) and the gas-phase temperature adjacent to the radial oxidizer-fuel interface. The spike occurs because of the exothermic reactions on the AP side of the interface and the endothermic reaction on the PBAA side. This spike results in both a high pyrolysis rate at $r=R_f$, as well as a pronounced gas-phase reaction rate near the circumference of the interface region. As evident from Fig. 11, the spike occurs at a later time than the onset of ignition based upon the previously mentioned ignition criteria. However, the predicted trend of ignition delay will not be influenced by selection of this ignition criterion.

It should be noted that the predicted surface temperature at the onset of ignition is about 450 K, which is considerably lower than that observed for steady-state burning. This is reasonable because of the time lag between the onset of ignition and steady-state burning. If the program were allowed to run longer, until steady-state conditions are reached, it is believed that the surface temperature would approach the steady-state value. The increase in surface temperature can be seen in Fig. 11.

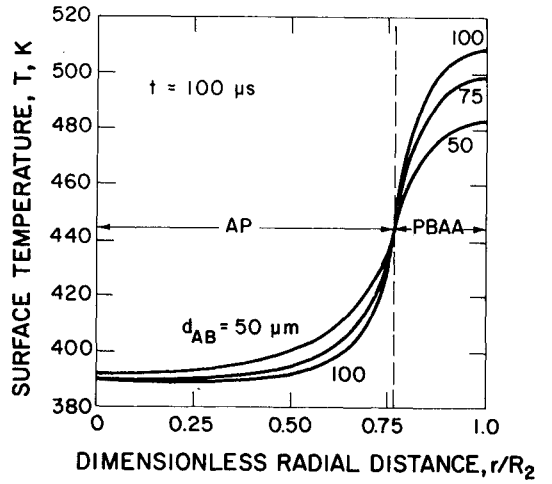

Fig. 12 Effect of AP particle size on radial variation of surface temperature (average $dP/dt = 120$ GPa/s).

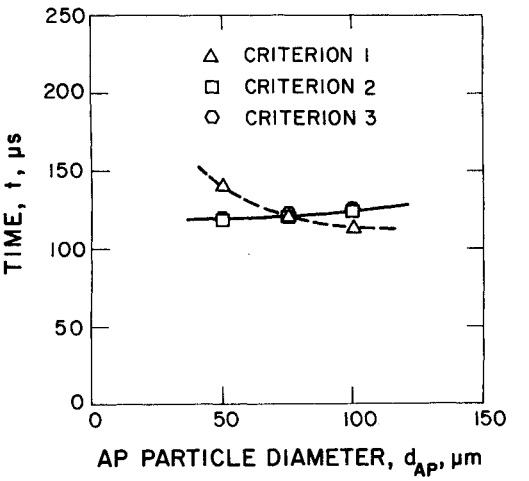

Fig. 13 Predicted effect of AP particle size on ignition delays using different ignition criteria based upon the attainment of: 1) $\dot{q}'''_{max,\,critical}$, 2) $r_{b,\,critical}$, and 3) zero axial velocity in the gas phase at a specified location (average $dP/dt = 120$ GPa/s).

Figure 12 shows the effect of AP-particle size on radial surface temperature distribution in the solid. As the AP-particle size is decreased, the radial temperature distribution becomes more uniform (i.e., the difference between the average AP and PBAA temperatures becomes smaller). This is reasonable because the lateral heat conduction is more pronounced for smaller particle sizes. In the limiting case, as the AP-particle size becomes vanishingly small, the temperature distribution will be uniform. Ignition criteria based upon AP burning rate (IC 2) or zero gas-phase velocity (IC 3) will result in lower ignition delay time for smaller AP particle sizes, since the surface temperature of AP is higher for smaller particles. On the other hand, since the surface temperature of PBAA is lower for smaller AP particle sizes, the adjacent gas-phase temperature is lower than that of a larger particle. Since pyrolyzed oxidizer species can diffuse readily to the higher temperature region over the PBAA surface, the maximum rate of gas-phase heat release occurs there. As a result, for smaller AP particles, the ignition criterion based upon maximum gas-phase heat release (IC 1) will show a longer ignition delay time, which is the opposite of that predicted by the other two criteria (see Fig. 13). However, the predicted ignition delay times appear to be relatively insensitive to the oxidizer particle size. Since the predicted ignition delay times

are more strongly dependent upon the properties of the fuel and oxidizer as well as the chemical kinetic constants, no conclusions can be drawn at this time as to the effect of oxidizer particle size on ignition delay.

It should be pointed out that, although the effect of oxidizer particle size does not appear to be important in the range studied, it does not mean that the two-dimensionality of the propellant can be ignored. The results clearly demonstrate the two-dimensionality of the process. The relative insensitivity of the predicted ignition delay on AP-particle size is caused mainly by the gas-phase reaction near the AP-binder interface.

Summary and Conclusions

A comprehensive theoretical model has been developed for the ignition of AP/PBAA composite solid propellants under rapid pressure loading. Important features of the model are: 1) two-dimensional (axisymmetric) geometry, allowing a more complete description of heterogeneous propellant ignition; 2) consideration of detailed chemical kinetics information; 3) inclusion of the pressurization (dP/dt) term in the governing equation for gases surrounding the propellant in order to simulate actual rocket motor ignition conditions or early phase of deflagration-to-detonation transition; and 4) no a priori assumption of the ignition site. Chemical reactions are allowed in all regions, including gas phase, interfaces, and subsurface. The governing equations were solved numerically using an implicit finite difference scheme with variable mesh size.

Important conclusions of this study are as follows:

1) The solutions revealed that the ignition process consists of the following sequence of events: a) as pressurization begins, the gas-phase temperature starts to rise, the unburned species near the propellant surface react, and heat is transferred to the propellant surface; b) following a period of inert heating and continued pressurization, the surface temperature rises and the solid-phase oxidizer and fuel pyrolyze; and c) when the concentration of gas-phase oxidizer, fuel species, and local gas-phase temperature are sufficiently high, intense gas-phase reactions begin. Ignition is defined as the attainment of a high reaction rate and, simultaneously a high surface pyrolysis rate.

2) Calculated ignition delay time based on several criteria (namely, attainment of a critical volumetric gas-phase heat release rate, a critical pyrolysis rate, and zero axial velocity in the gas-phase near the propellant surface) are in agreement with the experimentally observed trend that ignition delay time decreases with increasing pressurization rate. Predicted values of ignition delay for lower pressurization rates showed greater dependence on the choice of ignition criterion.

3) Solutions revealed significant temperature nonuniformity, implying two-dimensional effects that must be included in modeling composite propellant ignition. Although the ignition delay times appear to be relatively insensitive to the oxidizer particle size, this does not mean that two-dimensional effects are not important since the temperature profiles are highly nonuniform.

4) More accurate chemical kinetic constants pertaining to ignition are needed to describe the pyrolysis and gas-phase reactions for more precise prediction of ignition delay times. The kinetic constants for steady-state combustion may not be the same as those for ignition.

Acknowledgment

This paper represents a part of the work performed under the Contract N00014-79-C-0762, sponsored by the Power Program, Office of Naval Research, Arlington, Va., under the management of Dr. R. S. Miller.

References

[1]Kumar, M., Kuo, K. K., Kulkarni, A. K., and Wills, J. E., "Ignition of Composite Propellants under Rapid Pressure Loading," Annual Report to Office of Naval Research, Arlington, Va., Sept. 1981.

[2]Kumar, M., Wills, J. E., Kulkarni, A. K., and Kuo, K. K., "Ignition of Composite Propellants in a Stagnation Region under Rapid Pressure Loading," *Nineteenth Symposium (International) on Combustion*, The Combustion Institute, Pittsburgh, Pa., 1982, pp. 757-767.

[3]Price, E. W., Bradley, H. H. Jr., Dehority, G. L., and Ibiricu, M. M., "Theory of Ignition of Solid Propellants," *AIAA Journal*, Vol. 4, Sept. 1966, pp. 1153-1181.

[4]Kulkarni, A. K., Kumar, M., and Kuo, K. K., "Review of Solid Propellant Ignition Studies," AIAA Paper 80-1210, July 1980; also, *AIAA Journal*, Vol. 20, Feb. 1982, p. 243.

[5]Bradley, H. H. Jr., "A Unified Theory of Solid Propellant Ignition," Naval Weapons Center, China Lake, Calif., Rept. NWC TP 5618, Pts. 1-3, Dec. 1975.

[6]Kumar, R. K. and Hermance, C. E., "Gas Phase Ignition Theory of a Heterogeneous Solid Propellant," *Combustion Science and Technology*, Vol. 4, 1972, pp. 191-196.

[7]Kumar, M. and Kuo, K. K., "Ignition of Solid Propellant Crack Tip under Rapid Pressurization," *AIAA Journal*, Vol. 18, July 1980, pp. 825-833.

[8]Ohlemiller, T. J. and Summerfield, M., "A Critical Analysis of Arc Image Ignition of Solid Propellants," *AIAA Journal*, Vol. 6, May 1968, pp. 878-886.

[9]Lengelle, G., Brulard, J., and Montet, H., "Combustion Mechanisms of Composite Solid Propellants," *Sixteenth Symposium (International) on Combustion*, The Combustion Institute, Pittsburgh, Pa., 1976, pp. 1257-1269.

[10]Kishore, K. and Gayathri, V., "Chemistry of Ignition and Combustion of Ammonium Perchlorate Based Propellants," AIAA Progress in Astonautics and Aeronautics, *Fundamentals of Combustion of Solid Propellants*, edited by K. K. Kuo and M. Summerfield, to be published.

[11]Guirao, C. and Williams, F. A., "A Model for Ammonium Perchlorate Deflagration between 20 and 100 atm," *AIAA Journal*, Vol. 9, July 1971, pp. 1345-1356.

[12]Beckstead, M. W., Derr, R. L., and Price, C. F., "A Model for Composite Solid-Propellant Combustion Based on Multiple Flames," *AIAA Journal*, Vol. 8, Dec. 1970, pp. 2200-2207.

[13]Pearson, G. S., "Perchlorate Oxidizer," *Oxidation and Combustion Reviews*, Vol. 4, 1969, pp. 1-92.

[14]Jacobs, P. W. M. and Whitehead, H. M., "Decomposition and Combustion of Ammonium Perchlorate," *Chemical Reveiws*, Vol. 69, Aug. 1969, pp. 551-590.

[15]Ninan, K. N. and Krishnan, K., "Thermal Decomposition Kinetics of Polybutadiene Binders," *Journal of Spacecraft and Rockets*, Vol. 19, Jan.-Feb. 1982, pp. 92-94.

[16]Varney, A. M. and Strahle, W. C., "Thermal Decompositon Studies of Some Solid Propellant Binders," *Combustion and Flame*, Vol. 16, 1971, pp. 1-7.

[17]Allen, D. N. de G., *Relaxation Methods*, McGraw Hill Book Co., New York, 1954.

[18]Rosser, W. A. Jr., Inami, S. H., and Wise, H., "Thermal Diffusivity of Ammonium Perchlorate," *AIAA Journal*, Vol. 4, April 1966, pp. 663-666.

[19]Gordon, S. and McBride, B. J., "Computer Program for Calculation of Complex Chemical Equilibrium Compositions, Rocket Performance, Incident and Reflected Shocks, and Chapman-Jouguet Detonations," NASA SP-273, 1971, and Interim Revision, March 1976.